Chapter

Nanostructuring Indium-Tin-Oxide Thin Films by Femtosecond Laser Processing

Phuoc Huu Le and Chih-Wei Luo

Abstract

This chapter reviews the nanostructuring fabrications and properties of indium-tin-oxide (ITO) thin films by femtosecond laser annealing. Fundamental mechanisms of laser-induced periodic surface structures (LIPSS) and other nanostructures on ITO films are presented and discussed in detail. ITO films with large-area surface ripple structures with a multiperiodic spacing of ~800, ~400, and ~200 nm were successfully fabricated by femtosecond laser pulses, without scanning. The ITO films exhibited significant enhancement in electrical conductivity by ~30 times because of the formation and distribution of indium metal-like clusters. This metallic content of the laser-induced nanodots and nanolines further causes the anisotropic transmission characteristics in the visible range. In addition, by varying the laser fluences, nanostructures with cotton, brick, and ripple forms are generated on the surface of ITO films, which produce cyan, yellow, and orange colors. Intriguingly, the ITO films with laser-induced nanostructures can significantly attenuate blue light, thus they are potential for applications such as eye protection and information security.

Keywords: indium-tin-oxide (ITO), femtosecond laser annealing, laser-induced periodic surface structures (LIPSS), anisotropic transmission, laser-colorized ITO film

1. Introduction

Transparent conducting oxide (TCO) film is one of the essential components in various state-of-the-art optoelectronic devices, including liquid crystal displays (LCDs), organic solar cells, touch screens, and organic light emitting devices (OLEDs). Among TCOs, indium-tin-oxide (ITO) is a well-known wide bandgap semiconductor that has metal-like electrical properties and high optical transmission in the visible region [1, 2]. Indeed, ITO possesses high electrical conductivity (~10^{-4} Ω-cm) and high transmission (~90%) in the visible range [3, 4]. In OLED applications, surface properties of ITO films, such as their electron affinity and work function, play a key role in determining the characteristics of OLEDs, owing to their direct contact with the organic materials, as a hole injection layer [5]. ITO has also been extensively used as a good ohmic contact material owing to the excellent surface conductivity in GaN-base light emitting diodes (LEDs) [6].

Recently, material processing by femtosecond (fs) laser irradiation has attracted a great deal of attention because the energy of fs pulses can be precisely and rapidly transferred to the film without thermal effects. This is so-called femtosecond laser annealing (FLA). FLA demonstrates as a good method to induce crystallization within a thin layer of materials and avoid thermal melting in materials. Thus, FLA can be employed in flexible technology, where thin films are coated on polymer substrates with low glass transition temperature (T_g). For example, Pan et al. reported near-infrared femtosecond laser-induced crystallization in amorphous silicon [7]. Recently, laser-induced periodic surfaces structures (LIPSS) or ripples have been observed for various materials, under pulsed laser illumination near their ablation thresholds [8–14]. Materials with LIPSSs also possess modified physical properties, such as the friction [15], the hydrophobicity/hydrophilicity [16], the conductivity [11–13] and the absorptance [16–18].

This chapter reviews recent advances on fabrication of various nanostructures on the surface of ITO films by using femtosecond laser processing. In addition, it reports detailed property modification of fs-laser treated ITO films, including enhanced electrical conductivity, anisotropic optical transmission, laser-colorized effect, and performance of the organic photovoltaic devices using ITO with LIPSSs. This chapter also gives an insight into the formation mechanisms for LIPSSs, the relationship between fs-laser processing and properties of fs laser-treated ITO films, and potential applications of nanostructuring ITO films.

2. Fabrication and characterizations of nanostructuring indium-tin-oxide films

2.1 ITO thin film preparation

ITO thin films were deposited on a glass (a size of 1 × 1 cm) using magnetron sputtering deposition at room temperature, $O_2/(Ar + O_2)$ flow ratio of 0.047, and a power of 1000 W. The ITO target (58 × 15 cm) was composed of In_2O_3 with 10 wt% SnO_2. The as-deposited ITO thin films have a thickness of 30–80 nm and a resistivity of $\sim 4 \times 10^{-2}$ Ω-cm.

2.2 Experimental setups

For fabricating nanostructures, the ITO films were irradiated using a regenerative-amplified Ti:sapphire laser (Legend USP, Coherent), with a central wavelength of 800 nm, a pulse duration of 100 fs, a pulse energy of ~0.5 mJ, and a repetition rate of 5 kHz (**Figure 1a**). The diameter of the laser beam was adjusted to ~14 mm, which can cover fully the sample size of 1 × 1 cm. The samples were irradiated with different fs laser shots (N) of 0, 5×10^3, 2.5×10^4, 1×10^5, 3×10^5, and 3×10^6.

For studying the anisotropic optical transmission of nanostructured ITO films, all optical spectra were measured through an iris with a 0.1-mm-diameter hole located at a position close to the central region of the laser-induced nanostructures (or laser spot). The fs laser-treated ITO films had ripple structures of nanodots and nanolines on the film surfaces. The transmission spectra of the films were measured using polarized light with a direction of polarization (P) parallel or perpendicular to the direction of the long axis of the nanodots or nanolines (L) on the ITO films (see **Figure 1b** and the inset of **Figure 6c**).

For fabricating the various surface modifications in Section 5, the ITO films with a thickness of 80 nm were mounted on an xyz stage and irradiated at room temperature and ambient pressure using a commercial Ti:sapphire amplifier (Solstice Ace,

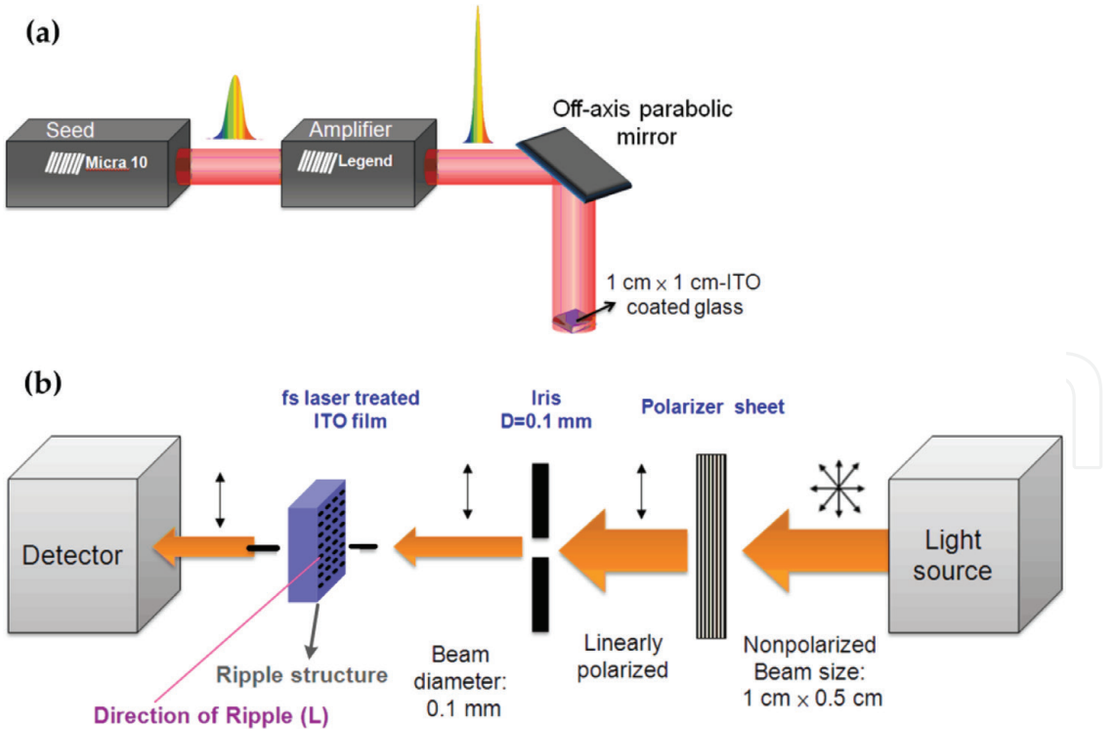

Figure 1.
Experimental setup for (a) the fabrication of nanostructuring ITO films and (b) the characterizations of anisotropic optical properties on ITO films with periodic nanostructures on the surfaces.

Spectra-Physics) with a central wavelength of 800 nm, a pulse duration of 35 fs, and a repetition rate of 2 kHz. The laser beam with line spot (a length of 4.6 mm and a width of 21 μm) was focused by a cylindrical lens (f = 40 mm). The scanning speed was approximately 160 μm/s.

2.3 Characterizations

The optical transmission of as-deposited and fs laser-treated ITO films was measured using an UV-visible-near-IR spectrophotometer (Shimadzu SolidSpec-3700). The morphology of the films was examined using a scanning electron microscope (SEM) (HITACHI-S2500 JSM-6500F). The film thicknesses were determined by surface contour measurement (KOSAKA ET4000A), with a vertical resolution of 0.1 nm. The resistivity, carrier concentration, and the Hall mobility of the ITO films were measured by the Hall measurements (Bio-Rad Microscience HL5500) using the Van der Pauw method. The surface composition and chemical bonding were studied by X-ray photoelectron spectroscopy (XPS, PHI Quantera AES 650), with source of Al Kα at 1486.7 eV, passing an energy of 15 keV, and analyzed a spot size of 100 μm. The XPS spectra were calibrated by using Au at binding energy of 84.0 eV. XPS curve fitting was performed using free-ware XPSPEAK4.1 from Dr. R.M. Kwok, the Shirley background subtraction, and assuming a Gaussian-Lorentzian peak shape. Auger electron spectroscopy (AES, ULVAC-PHI 700) with a spatial resolution of ~30 nm under 5 keV operating voltage was used to study the local compositions of the as-deposited and fs laser-irradiated ITO films.

In Section 5, the morphology of the colorized ITO films was measured using high resolution field emission SEM (JEOL). To determine the relationship between the reflectance/transmittance spectra and the colors of fs laser-colorized ITO films, we used a spectrometer (U3310, Hitachi) with both deuterium and tungsten iodide lamps (allowing for a scanning range from 190 to 900 nm with a resolution of 0.3 nm).

3. Superior local conductivity in self-organized nanodots on indium-tin-oxide films induced by femtosecond laser pulses

Figure 2a–f shows the surface morphology of ITO films after normal-incidence irradiation with different pulse numbers from 0 to 5×10^3 (fluence: 0.1 mJ/cm^2). The film only exhibits few small dots for $N = 5 \times 10^3$ shots (**Figure 2b**). Meanwhile, the laser-induced periodic structure is clearly observed on the surface of ITO films for $N \geq 2.5 \times 10^4$ shots (**Figure 2c–f**). In the inset of **Figure 2f**, the submicron ripple structure is composed of self-organized line dots (size: 20–500 nm). The periodic ripple pattern has long axis perpendicular to the direction of the laser polarization (the arrow in **Figure 2f**). The mixture of the dotted and ripple structures is attributed to the interference of scattered and diffracted waves at the grains and/or defects. This is similar to ordered YBCO array structures, formed by the solidification of melted dot patterns, under conditions of constructive interference and minimized surface energy [11, 19].

The present periodic ripple structures have spacing of approximately 798 ± 15, 420 ± 14, and 230 ± 15 nm. The formation of the two large ripple spacing cases (i.e., 798 ± 15 and 420 ± 14 nm) can be easily explained by classical scattering model [20]:

$$\Lambda = \frac{\lambda}{1 \pm \sin\theta} \tag{1}$$

where Λ is the ripple spacing, λ is the laser wavelength, and θ is the incident angle of the laser beam onto the target. However, the classical scattering model with Eq. (1) cannot be used to predict for the shorter ripple spacing of 230 ± 15 nm, which is much smaller than the laser wavelength of 800 nm. We noted that the spacing value is close to ~200 nm, thus it could be induced by second harmonic generation (SHG) with a shorter wavelength of 400 nm around the surface of ITO film. It is reasonable for occurring SHG owing to the surface asymmetry when the subwavelength ripple with ~200 nm is indeed observed in high intensity regions, especially in the center of laser Gaussian beam (**Figure 2f**).

Figure 3 shows the effects of number of pulses (N) from 0 to 3×10^6 shots on the carrier concentration (n), carrier mobility (μ), and resistivity (ρ) of the ITO films. For $N \leq 10^3$, the laser-treated ITO films almost remain the same as that of the as-deposited ITO films. As further increasing N from 5×10^3 to 3×10^6, the n increases noticeably from ~1×10^{19} to ~1.6×10^{19} cm^{-3}. In contrast, the μ decreases correspondingly from 12.3 to 10.2 cm^2/V-s (i.e., 17% reduction), after fs laser annealing with 3×10^6 shots at a fluence of 0.1 mJ/cm^2. Reasonably, by using the Hall measurement, it is hard to detect a slight difference in n for $N \leq 10^3$. However, for larger N (>10^3 shots), the accumulated number of pulses induces the thicker laser-irradiated area for detecting the variation in n using the Hall measurement. Due to the aforementioned variation of n and μ, the resistivity presents a 14% reduction from 4.3×10^{-2} at $N = 0$ to 3.7×10^{-2} Ω-cm for $N = 3 \times 10^6$ shots, which is primarily due to the increased n. Noticeably, the thickness the ITO films before and after irradiation are 30 ± 1.5 nm, and the thickness variation is not noticeable, and thus, the effect of thickness on the electrical properties can be eliminated.

The optical transmittance of the as-deposited ITO and fs-laser treated ITO films for 3×10^5 and 3×10^6 shots is shown in **Figure 3b**. Obviously, the optical transmittance of fs laser-treated ITO films remains about the same as that of the as-deposited ITO film, and they achieve a high transmittance of approximately 85% in the visible to near-infrared (NIR) range. The electrical and optical results indicate that fs laser annealing represents a new method to enhance the electrical properties of ITO films and retain their high optical transmittance.

To identify the cause of surface conductivity enhancement for fs laser-treated ITO films, we performed the X-ray photoelectron spectroscopy (XPS) experiments

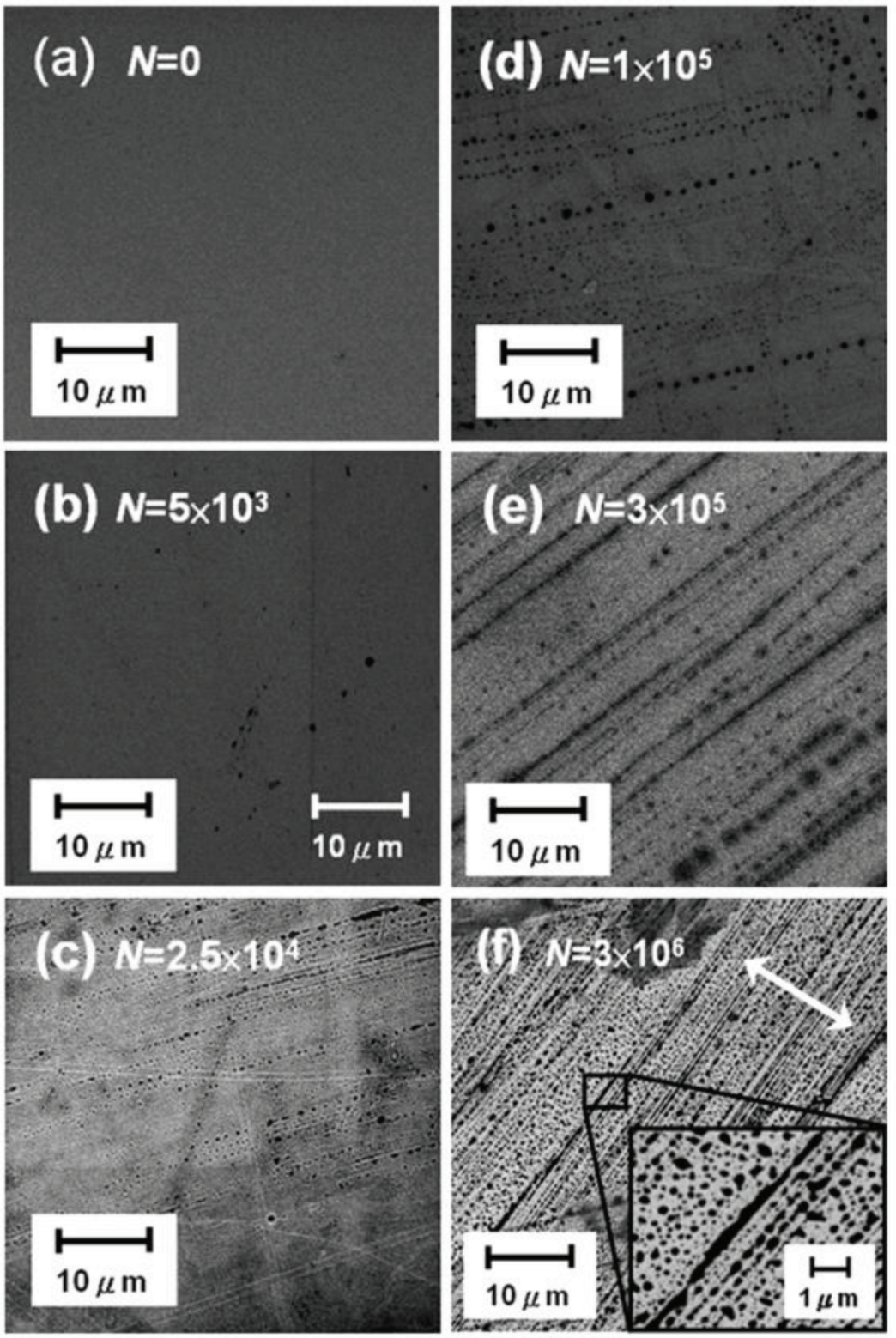

Figure 2.
(a–f) SEM images of periodic surface structures induced by 800 nm fs laser pulses at a fluence of 0.1 mJ/cm² and with various pulse numbers (N = 0, 5 × 10³, 2.5 × 10⁴, 1 × 10⁵, 3 × 10⁵, and 3 × 10⁶, respectively). The black-square inset shows the enlarged surface features at corresponding locations in (f). The arrow indicates the direction of the laser polarization [11].

on the as-deposited and fs laser-treated ITO films in comparison with In_2O_3 powder. **Figure 4a** shows Donley's model of surface composition of an ITO film, which has In_2O_3-like sites, oxygen-deficient sites, and hydroxide and oxyhydroxide groups [21]. **Figure 4d–g** shows the O1s XPS spectra of fs laser-treated ITO films with N from 5×10^3 to 3×10^6. **Figure 4c** presents the O1s XPS spectrum of

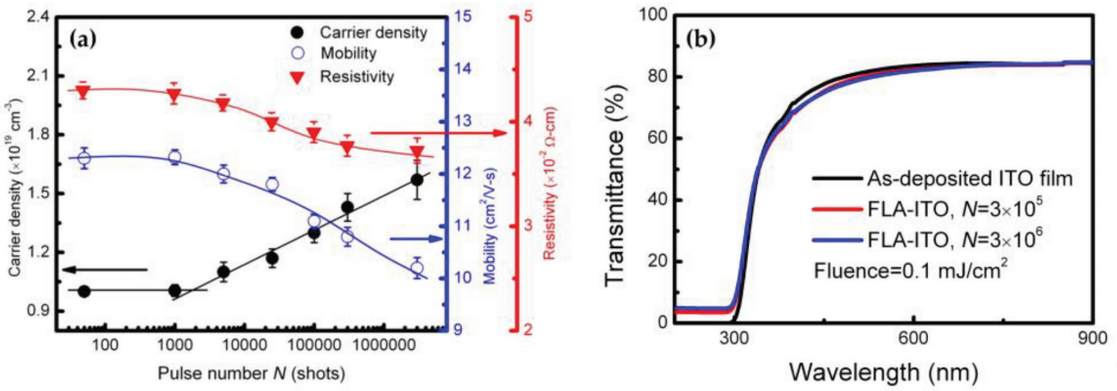

Figure 3.
(a) The carrier concentration, mobility, and resistivity in the fs laser-treated ITO films as a function of the pulse numbers (the solid lines are a guide to the eyes). (b) The transmittance in the fs laser-treated ITO films as a function of wavelengths with various pulse numbers (N = 0, 3 × 10^5, and 3 × 10^6, respectively) at a fluence of 0.1 mJ/cm^2 [11].

as-deposited ITO films. It can be fitted well with three peaks, namely the In_2O_3-like oxygen at 529.6 ± 0.1 eV [21, 22], oxygen adjacent to the oxygen-deficient sites at 531.0 ± 0.1 eV [21, 22], and hydroxide and/or oxyhydroxide peak at 532.0 ± 0.1 eV [21–23]. Compared with a reference sample of In_2O_3 powder (**Figure 4b**), the oxygen peak (at 531.0 ± 0.1 eV) that is adjacent to the oxygen-deficient sites of as-deposited ITO film (**Figure 4c**) increases because of the formation of oxygen vacancies during the thin film growth using sputtering [23].

Furthermore, the XPS spectra of In $3d_{5/2}$, for In metals, In_2O_3 powders, and fs laser-treated ITO films, are shown in **Figure 5a**. The In $3d_{5/2}$ peak of In metal locates at a lower binding energy of 443.7 eV, corresponding to the In bonding state of In-In bonds [23]. However, the In $3d_{5/2}$ peak of the In_2O_3 powder shifts to the higher binding energy of 444.6 eV, corresponding to the In^{3+} bonding state of In_2O_3 [22, 24]. Thus, the valence states of In_2O_3 for the as-deposited ITO film can be demonstrated by the In $3d_{5/2}$ peak at 444.4 eV. As increasing the number of fs laser pulses, there is a gradual shift in the In $3d_{5/2}$ peak from the In-O bonding state to In-In bonding state. Particularly, the peak of In $3d_{5/2}$ for $N = 3 \times 10^6$ is located at 443.9 eV, which is close to the binding energy of In-In bonds. This result strongly indicates that the existence of In metal-like clusters on the surfaces of fs laser-treated ITO films, particularly inside the self-organized nanodots that result in the enhanced electrical conductivity for the films. Similarly, upon fs laser irradiation, the aggregation of metal nanoparticles was observed in thin plasma polymer films due to the strong interaction via dipolar forces of the metals [25].

Figure 5b summarizes the findings that periodic self-organized nanodots are formed on the surfaces of the ITO films treated by fs laser pulses because of constructive interference of fs laser. The nanodots are In-like clusters, which induce superior local surface conductivity, and consequently offer reducing the electrical resistivity for the films. The approach for finding the self-organized nanodots with superior local surface conductivity may be suitable for applications such as nanolithography, nanophotoelectrons, and nanomechanics, in large-area nanotechnology.

In brief, periodic ripple structures with a multiperiodic spacing of ~800, ~400, and ~200 nm were successfully fabricated by fs laser pulse irradiation. The ripple structure is composed of self-organized nanodots with a size of 20–500 nm, which are presumably formed by the solidification of melted dot patterns, under conditions of constructive interference and minimized surface energy. The ITO films with ripple structures on the surfaces exhibited significant enhancement in electrical conductivity, which is attributed to the formation of In metal-like nanodots/clusters.

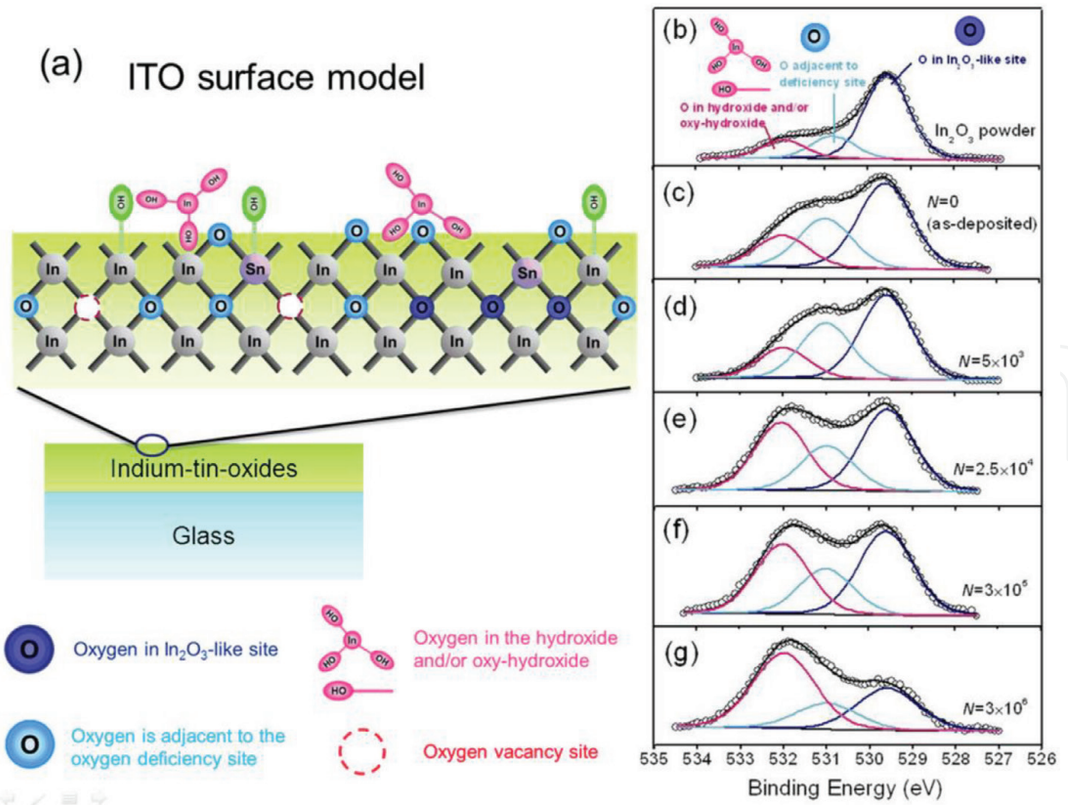

Figure 4.
(a) Schematic representation of as-deposited ITO surface composition based on Donley's model [21]. (b) The O1s XPS spectra of In_2O_3 powder and fs laser-treated ITO films with various pulse numbers (N = 0, 5 × 10^3, 2.5 × 10^4, 3 × 10^5, and 3 × 10^6, respectively) [11].

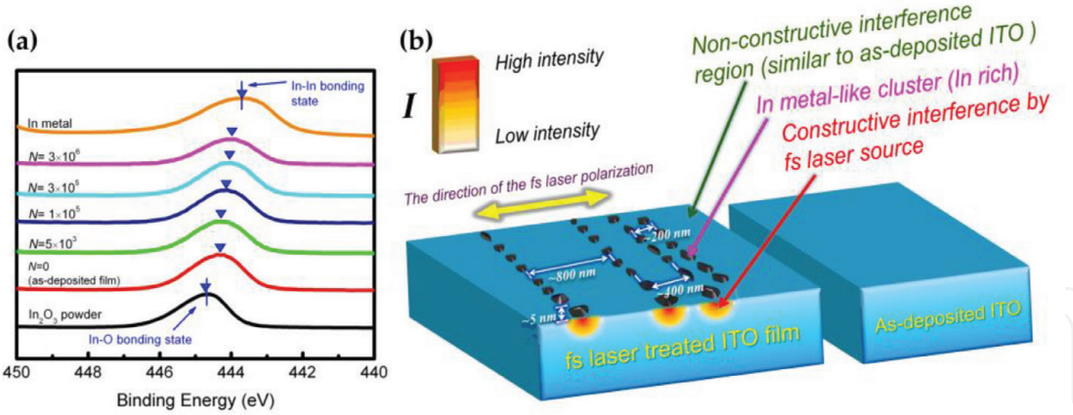

Figure 5.
(a) The In $3d_{5/2}$ XPS spectra of In_2O_3 powder, In metal, and fs laser-treated ITO films with various pulse numbers (N = 0, 5 × 10^3, 1 × 10^5, 3 × 10^5, and 3 × 10^6, respectively). (b) A schematic illustration for the formation of self-organized nanodots induced by the constructive interference of fs laser at near-surface region. The dot is composed of In-rich clusters with a height of ~5 nm as a result of In-O bonding breaking into In-In under local-field enhancement [11].

4. Anisotropic optical transmission of femtosecond laser-induced periodic surface nanostructures on indium-tin-oxide films

This section focuses on the anisotropic optical properties of the nanostructures, including nanodots and nanolines, on ITO films fabricated by fs laser irradiation [12]. **Figure 6a** and **b** shows the surface morphology of nanodots and nanolines on ITO films. The solid line in **Figure 6c** presents the optical transmission of an

as-deposited ITO film in the visible range of nonpolarized light. The transmission spectra of the fs laser-treated ITO films were measured using polarized light with L//P or L⊥P, as shown in **Figure 6e**. The transmission of L//P ($T_{L//P}$) for visible light was lower than that of L⊥P ($T_{L\perp P}$) in the ITO films with structures of nanodots and nanolines in which the nanoline structure exhibited larger difference between the transmittances of $T_{L//P}$ and $T_{L\perp P}$ in visible range than that of nanodot structure. Indeed, the extinction ratio ($T_{L\perp P}/T_{L//P}$) in the nanoline film was enhanced by 42% at a wavelength of 400 nm (**Figure 6d**). The laser-induced periodic nanostructures on the film surfaces induced this dichroic or anisotropic transmission property for the fs laser-treated ITO films.

A schematic illustration for the dichroic optical property of the nanoline film is shown in the inset of **Figure 6c**. The vertically polarized light (P_V), which is parallel to the long axis of the nanoline structure (L), was significantly blocked by the nanostructured ITO films. Meanwhile, the horizontally polarized light (P_H) can pass through the nanoline structure, which is perpendicular to the long axis of the nanoline structure (L). These results demonstrate that anisotropic optical transmission can be simply induced and manipulated by using ITO films treated under fs laser irradiation. This property may have potential in applications such as optical devices for polarization control in the visible range [26]. We note that the anisotropic reflection property of the nanostructured ITO films was not evident because the films had a relatively low reflectance compared to the transmittance.

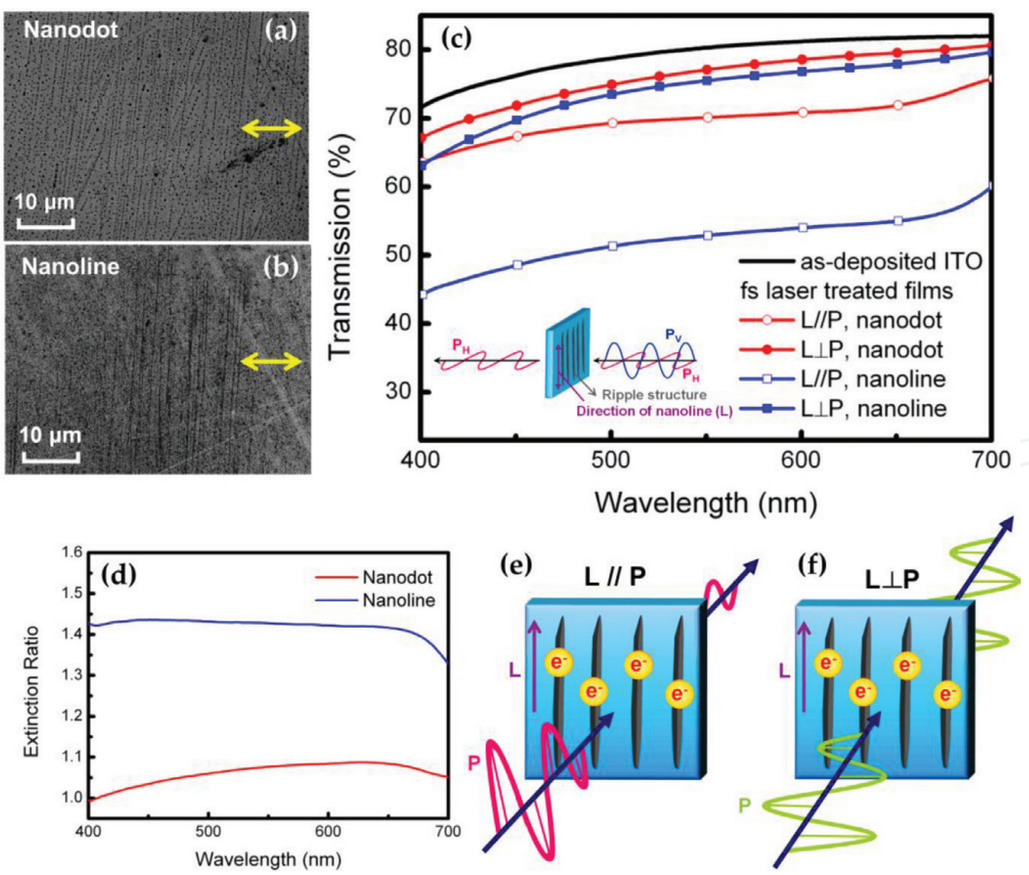

Figure 6.
(a and b) SEM images of nanodots and nanolines on ITO films. The arrows indicate the polarization direction of the irradiated fs laser. (c) The optical transmission spectra of as-deposited ITO and fs laser-treated films with the structures of nanodot and nanoline; the inset in (c) shows a schematic illustration of the two forms of polarized light (P_V and P_H) passing through a fs laser-treated ITO film. L: the directions of nanolines. (d) The extinction ratio ($T_{L\perp P}/T_{L//P}$) for the fs laser-treated films with structures of nanodot and nanoline. $T_{L\perp P}$ ($T_{L//P}$) is the transmittance in the configuration, L⊥P (L//P), as shown in (e) [12].

For the case of L//P in **Figure 6e**, the metallic and periodic nanoline structure on the ITO films reflects or absorbs the incoming electromagnetic (EM) wave due to the movement of electron along the metallic nanolines and Joule heating loss, consequently leading to blocking of the EM wave. However, the movement of electrons along the metallic nanolines is not in the same manner for the case of EM wave with L⊥P (**Figure 6f**). The loss caused by Joule heating and reflection is limited, and thus, the EM wave is transmitted highly through the ITO films with periodic nanodot or nanoline structures (**Figure 6f**).

To get an insight into the responsible mechanism for the anisotropic optical properties, the compositions of fs laser-treated ITO films were investigated using AES. **Figure 7a** shows the first derivative (*dN*/*dE*) AES peaks (i.e., In(MNN) at 410 eV, Sn(MNN) at 433 eV, and O(KLL) at 519 eV [27]) of an as-deposited film and a nanoline film. The point A (outside a nanoline) and point B (inside a nanoline) are shown by the SEM image in **Figure 7b**. Obviously, for the fs laser-treated ITO film, the *dN*/*dE* signals of In(MNN), Sn(MNN), and O(KLL) slightly reduced at point A as compared with those of as-deposited ITO film. Meanwhile, the *dN*/*dE* signals (top-pink line in **Figure 7a**) reduced remarkably at point B (inside a nanoline, see **Figure 7b**). The reduction in AES signals indicates that the composition of fs laser-treated ITO films is modified, especially at the nanoline locations. According to the results in the previous section and further examination [12], the surface compositions at nanodot and nanoline structures deviated from the stoichiometry of ITO and are metal-like area in particular. Consequently, the ITO films with a nanoline structure functioned as a grid of regular metallic wires, which induced the movement of electron along the metallic nanolines and Joule heating loss to block the EM wave for the case of L//P. However, the energy loss caused by Joule heating and reflection is limited for L⊥P because an EM wave cannot induce electron movement along the metallic nanolines in the same manner to result in high EM wave transmission. Since the total area of nanoline is larger than that of nanodot, the anisotropic optical property of the former is more critical than the latter [12].

In summary, the fs laser-treated ITO films with the structures of nanodot and nanoline on the surfaces possessed anisotropic optical transmission properties (i.e., $T_{L\perp P} > T_{L//P}$). The fs laser-treated ITO films may be applied to optoelectronics as the polarizing optical elements and smart window technology in the visible spectroscopy.

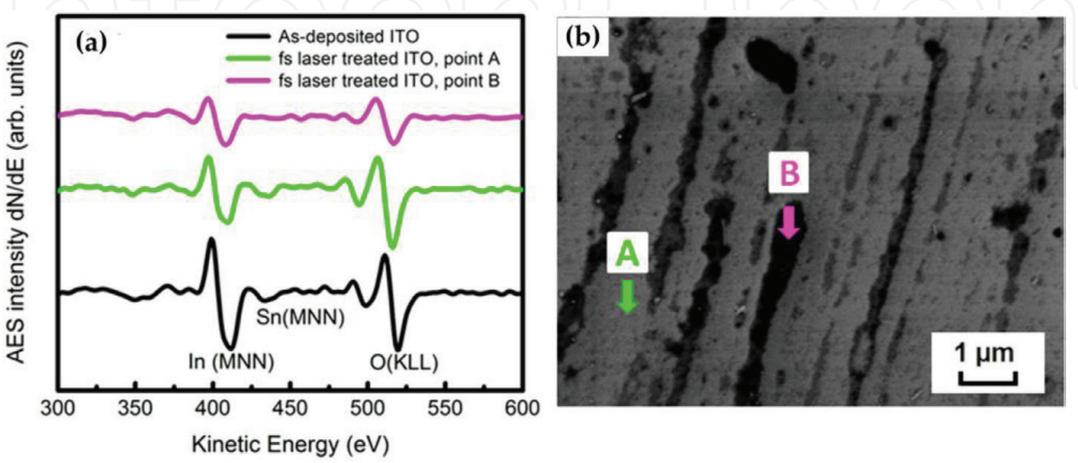

Figure 7.
(a) The first derivative (dN/dE) of AES peaks, In (MNN), Sn (MNN), and O (KLL), measured for an as-deposited ITO film and a fs laser-treated ITO film with a nanoline structure. The point A (outside a nanoline) and point B (inside a nanoline) correspond to the arrows marked in (b), the SEM image of a fs laser-treated ITO film [12].

5. Femtosecond laser-colorized indium-tin-oxide films for blue light attenuation and image screening

This section further demonstrates the development of various nanostructuring patterns on ITO films by fs laser annealing. **Figure 8** presents the surface morphology of an untreated ITO film and five laser-annealed ITO films. **Table 1** summarizes the experimental conditions and the nanostructures on the film surfaces. Differ from the flat surface of as-deposited ITO film in **Figure 8a**, the UDL-1 presents a densely cotton-like structure on the surface when the fluence of 646.1 mJ/cm^2 is employed (**Figure 8b**). By decreasing the laser fluence to 216.7 mJ/cm^2, the film has a brick-like structure. At a low fluence of 59.6 mJ/cm^2, a regular ripple structure (composed of nano-bricks) is obtained on the surface (**Figure 8f**). **Figure 8c–f** shows all of the ripple structures (formed by nano-bricks), which were fabricated by scanning a laser spot along the y-axis and parallel to the polarization of laser beam. The spatial period along the y-axis is much smaller than the wavelength of the radiation, which is the so-called high spatial frequency LIPSS (HSFL). Usually, in transparent materials, HSFLs are generated under hundreds to thousands of ultra-short laser pulses [28] perpendicular to the direction of laser polarization with a fluence below the damage threshold of materials [29]. With a scanning speed of ~12.5 pulses/μm and a spot size of 21 μm in width, the ITO films were irradiated by about 260 pulses at a single point. All laser-annealed ITO films obtained surface nanostructures with HSFLs.

For sample UDL-5 in **Figure 8f**, the nano-bricks exhibited a length of ~250 nm (along the x-axis) and a width of ~70 nm (along the y-axis), and they are regularly separated by around 500 nm along the x-axis. This 500-nm-period structure, so-called low spatial frequency LIPSS (LSFL), is parallel to the polarization of laser beam. Usually, LSFL is observed on the surface of dielectric materials. The spatial period can be estimated by $\Lambda_{\text{parallel}} = \lambda/n$, where n is the refractive index of

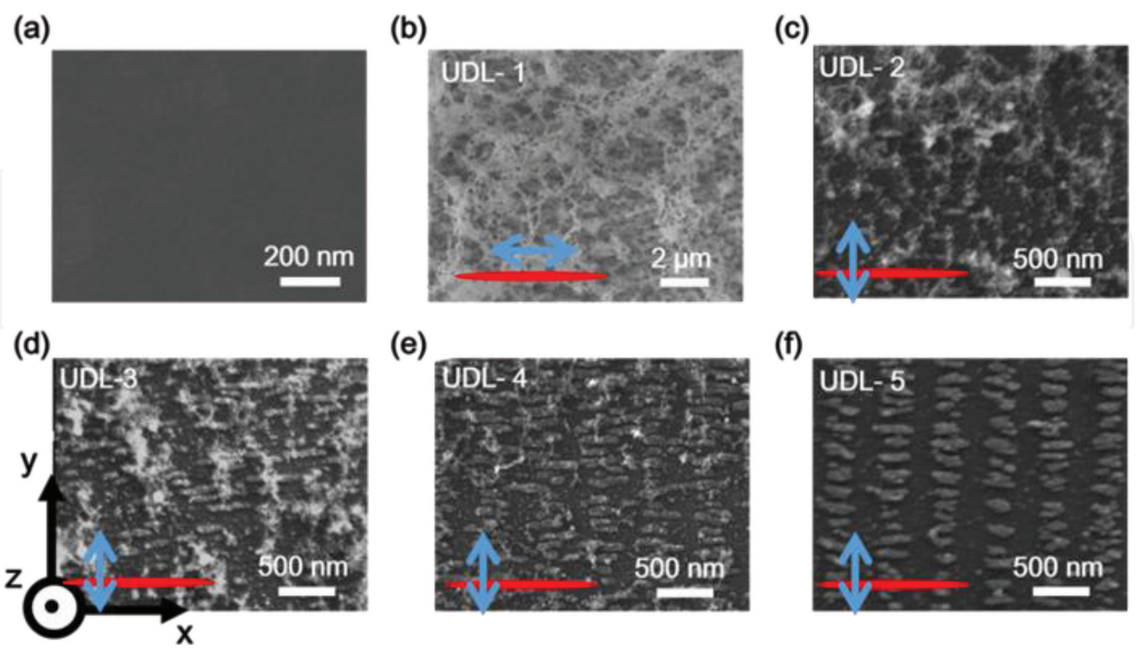

Figure 8.
SEM images showing the morphology of the ITO films before and after fs laser annealing. (a) The surface morphology of an untreated ITO film. (b) A laser-annealed ITO film (UDL-1, fluence = 646 mJ/cm^2) with scanning along the y-axis and polarization (blue arrow) parallel to the laser line-spot (red). (c–f) Laser-annealed ITO films [UDL-2 (fluence = 217 mJ/cm^2), UDL-3 (fluence = 197 mJ/cm^2), UDL-4 (fluence = 68 mJ/cm^2), and UDL-5 (fluence = 60 mJ/cm^2)] with scanning along the y-axis and polarization (blue arrow) perpendicular to the laser line-spot (red) [14].

Sample no.	Fluence (mJ/cm^2)	Nanostructure		Color
		Cotton-like structure	Brick-like structure	
UDL-1	646.1	V	—	Cyan
UDL-2	216.7	V	V	Yellow
UDL-3	197.0	V	V	Yellow
UDL-4	67.7	V	V	Orange
UDL-5	59.6	—	V	Orange

Table 1.
Laser fluence and the structure formation on the colorized ITO films.

the dielectric material, when the photon energy is smaller than the bandgap of the material [30]. The LIPSS theory of Sipe et al. for transparent materials has also predicted the spatial period of $\Lambda_{parallel} = \lambda/n$ that is attributed to radiation remnants [31]. Radiation remnants could be generated at the solid/air interface by absorbing photons from the incident radiation and then transfer to the materials at the associated spatial frequencies. Additionally, when the photon energy is smaller than the bandgap of the material, electrons can be excited to higher energy levels by absorbing multiple photons. In other words, laser provides a sufficient strong electric field to drive the electrons to tunneling out and consequently induces the ablation on the surface of materials. The bandgap for ITO is around 3.7 eV [32], and refractive index n is ~1.60 at 800 nm [33]. Here the photon energy of the irradiated laser is 1.55 eV, so it is estimated that $\Lambda_{parallel}$ = 500 nm, agreeing well with the experimental result for sample UDL-5.

Figure 9a shows the laser fluence dependence of the colors of laser-annealed ITO films. The untreated ITO film exhibits purple color, while laser-annealed ITO films become cyan, yellow, or orange, depending on the nanostructures on their surfaces. The reflectance and transmittance spectra of all ITO films in the visible region were measured to clarify the origin of laser-colorized ITO films. For an untreated ITO film, the reflectance is relatively high for wavelength ranges below 425 nm and above 650 nm (**Figure 9b**). Thus, the untreated ITO film is purple. Intriguingly, the reflectance spectra for the laser-annealed ITO films are significantly different. For high fluence (UDL-1), the reflectance spectrum in a range of 450–600 nm is substantially higher than that of the untreated ITO film, with a 2.2-fold increase at around 550 nm; meanwhile, the reflectance spectra below 400 nm and above 650 nm reduce remarkably. Therefore, the laser-colorized ITO film of UDL-1 is cyan. When the laser fluence reduces, the broad main peak in **Figure 9c** gradually shifts from 550 to 575 nm, and thus, the color changes from cyan to yellow and then to orange.

As shown in **Figure 9d**, all of the transmittance spectra for ITO films are reduced after fs laser annealing. Interestingly, the transmittance reduction in the region of 390–480 nm is significantly greater than that in long-wavelength region. It is worthy of mentioning that blue light is dominated in the region of 390–480 nm, and it has been demonstrated to cause damage to eyes [34]. Among the treated samples, UDL-5 sample treated under low fluence offers a larger reduction in the blue-light region and a smaller suppression in the red-light region. This study has demonstrated that the fs laser-colorized ITO films can be directly used for LCD displays in which the films maintain their original function as an electrode and act as a blue light filter to protect eyes.

When laser-colorized ITO films are used in the LCD displays, the image displayed on the LCD can be selectively screened by varying the view angle. **Figure 10a** shows the schematics for testing this concept. If the view angle θ is close to 0 (i.e.,

watching the panel normally), the image on the panel is normal. However, the image on the panel is blocked by the strong reflected light with colors that depend on view angle θ as watching the panel obliquely (**Figure 10b–e**). As a result, due to strong reflection of certain colors, the image on the panel cannot be seen. This finding is potential for information security and the protection of privacy [14].

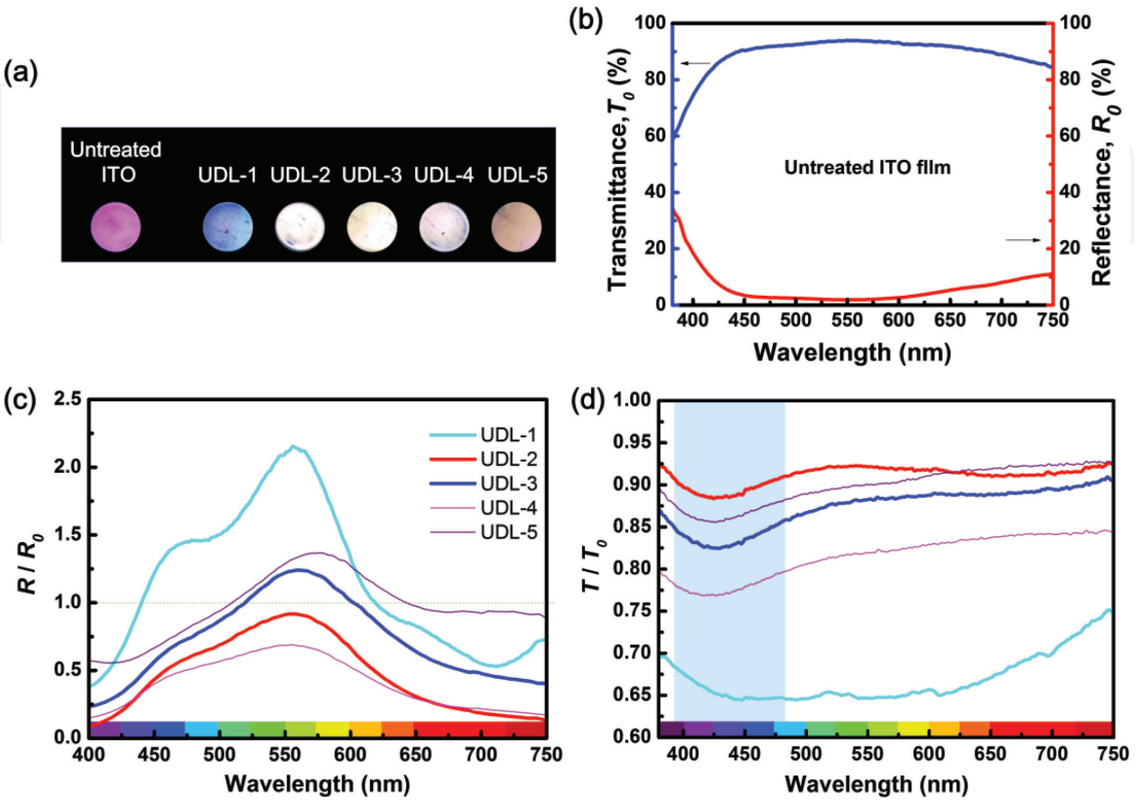

Figure 9.
(a) The colors of ITO films before and after fs laser annealing. (b) The reflectance (R_0) and transmittance (T_0) spectra for an ITO film before fs laser annealing. (c) The ratio of the reflectance spectra for the ITO films before (R_0) and after (R) fs laser annealing. (d) The ratio of the transmittance spectra for the ITO films before (T_0) and after (T) fs laser annealing. The blue-shaded area covers the wavelengths that cause damage to eyes [14].

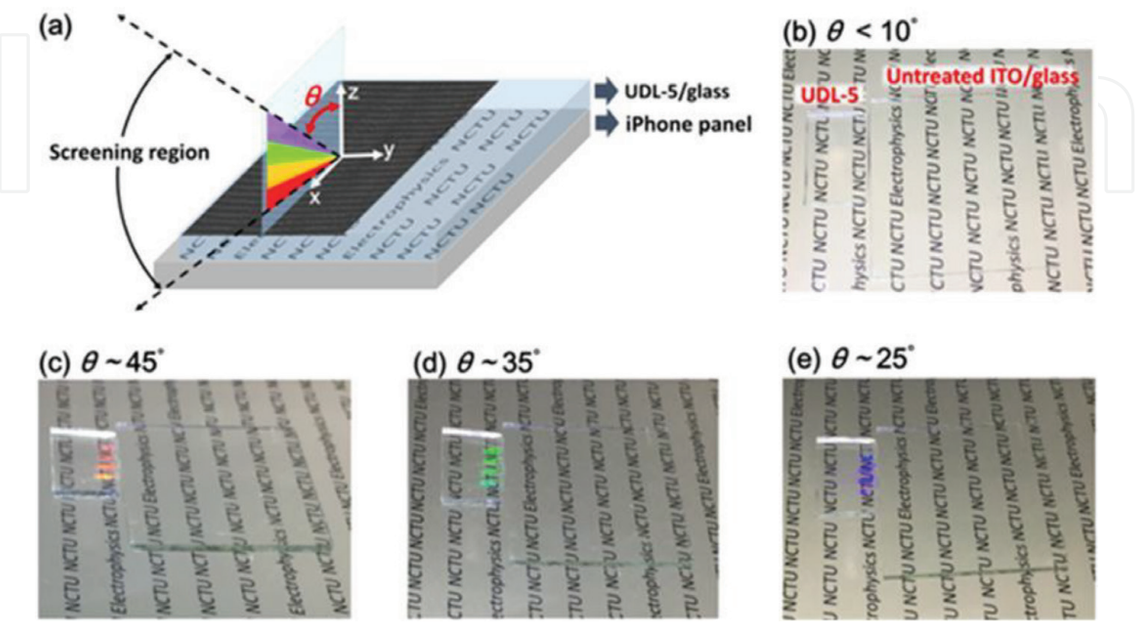

Figure 10.
(a) The schematics for capturing the images in (b–e), where θ is the view angle. (b–e) observing the image on a screen through an untreated ITO film and a laser-colorized ITO film (UDL-5) at various view angles [14].

6. Conclusions

In this chapter, we review the fabrications of various periodic nanostructures, that is, ripple structures of self-organized nanodots, nanolines, nano-cottons, and nano-bricks on the surfaces of ITO thin films after fs laser pulse irradiation. The ITO films with surface ripple structures were successfully prepared at a fluence of 0.1 mJ/cm^2 and numbers of pulses from 5 × 10^3 to 3 × 10^6, without scanning. The fs laser-annealed ITO films exhibited a great enhancement in electrical conductivity (~30 times) due to the presence of indium-like clusters in ripple structures. In addition, the ITO films obtained nanodot structure at a fluence of 0.1 mJ/cm^2 and a pulse number of 3 × 10^6 and nanoline structure at a fluence of 0.2 mJ/cm^2 and a pulse number of 2 × 10^7. The fs laser-annealed ITO films presented interesting anisotropic transmission properties ($T_{L\perp P} > T_{L//P}$) because the nanostructures functioned as a metallic grid that induced the electron movement along the nanolines and Joule heating loss to block the EM wave for the case of L//P (i.e., the direction of nanolines, L, is parallel to the polarization direction, P, of fs laser pulses). Moreover, nanostructures with cotton, brick, and ripple forms are generated on the surface of ITO films by controlling the laser fluences from 60 to 646 mJ/cm^2 and a scanning speed of ~12.5 pulses/μm, which produce cyan, yellow, and orange colors. These nanostructures can significantly attenuate blue light, and thus, they are possible for applications such as eye protection and information security.

Acknowledgements

This work was also supported by the Ministry of Science and Technology of the Republic of China, Taiwan (Grant nos. 107-2119-M-009-010-MY2, 106-2119-M-009-013-FS, and 106-2628-M-009-003-MY3). Besides, this work was financially supported by the Center for Emergent Functional Matter Science of National Chiao Tung University from the Featured Areas Research Center Program and the Research Team of Photonic Technologies and Intelligent Systems at NCTU within the framework of the Higher Education Sprout Project by the Ministry of Education (MOE) in Taiwan.

Author details

Phuoc Huu Le[1] and Chih-Wei Luo[2*]

1 Department of Physics and Biophysics, Faculty of Basic Sciences, Can Tho University of Medicine and Pharmacy, Can Tho, Vietnam

2 Department of Electrophysics, National Chiao Tung University, Hsinchu, Taiwan, Republic of China

*Address all correspondence to: cwluo@mail.nctu.edu.tw

References

[1] Kim CE, Yun I. Effects of nitrogen doping on device characteristics of InSnO thin film transistor. Applied Physics Letters. 2012;**100**:013501. DOI: 10.1063/1.3673556

[2] Zhao Y, Duan L, Zhang D, Hou L, Qiao J, Wang L, et al. Small molecular phosphorescent organic light-emitting diodes using a spin-coated hole blocking layer. Applied Physics Letters. 2012;**100**:083304. DOI: 10.1063/1.3688300

[3] Kim H, Gilmore CM, Piqué A, Horwitz JS, Mattoussi H, Murata H, et al. Electrical, optical, and structural properties of indium–tin–oxide thin films for organic light-emitting devices. Journal of Applied Physics. 1999;**86**:6451. DOI: 10.1063/1.371708

[4] Guillén C, Herrero J. Structure, optical, and electrical properties of indium tin oxide thin films prepared by sputtering at room temperature and annealed in air or nitrogen. Journal of Applied Physics. 2007;**101**:073514. DOI: 10.1063/1.2715539

[5] Wu CC, Wu CI, Sturm JC, Kahn A. Surface modification of indium tin oxide by plasma treatment: An effective method to improve the efficiency, brightness, and reliability of organic light emitting devices. Applied Physics Letters. 1997;**70**:1348-1350. DOI: 10.1063/1.118575

[6] Horng RH, Wuu DS, Lien YC, Lan WH. Low-resistance and high-transparency Ni/indium tin oxide ohmic contacts to p-type GaN. Applied Physics Letters. 2001;**79**:2925-2927. DOI: 10.1063/1.1415048

[7] Shieh J-M, Chen Z-H, Dai B-T, Wang Y-C, Zaitsev A, Pan C-L. Near-infrared femtosecond laser-induced crystallization of amorphous silicon. Applied Physics Letters. 2004;**85**:1232. DOI: 10.1063/1.1782267

[8] Huang M, Zhao F, Cheng Y, Xu N, Xu Z. Origin of laser-induced near-subwavelength ripples: Interference between surface plasmons and incident laser. ACS Nano. 2009;**3**:4062. DOI: 10.1021/nn900654v

[9] Zhao QZ, Malzer S, Wang LJ. Formation of subwavelength periodic structures on tungsten induced by ultrashort laser pulses. Optics Letters. 2007;**32**:1932-1934. DOI: 10.1364/OL.32.001932

[10] Jia X, Jia TQ, Zhang Y, Xiong PX, Feng DH, Sun ZR, et al. Periodic nanoripples in the surface and subsurface layers in ZnO irradiated by femtosecond laser pulses. Optics Letters. 2010;**35**:1248-1250. DOI: 10.1364/OL.35.001248

[11] Wang C, Wang HI, Tang WT, Luo CW, Kobayashi T, Leu J. Superior local conductivity in self-organized nanodots on indium-tin-oxide films induced by femtosecond laser pulses. Optics Express. 2011;**19**:24286-24297. DOI: 10.1364/OE.19.024286

[12] Wang C, Wang HI, Luo CW, Leu J. Anisotropic optical transmission of femtosecond laser induced periodic surface nanostructures on indium-tin-oxide films. Applied Physics Letters. 2012;**101**:101911. DOI: 10.1063/1.4751983

[13] Chen MH, Tseng YH, Chao YP, Tseng SY, Lin ZR, Chu HH, et al. Effects on organic photovoltaics using femtosecond-laser-treated indium tin oxides. ACS Applied Materials and Interfaces. 2016;**8**(**38**):24989-24993. DOI: 10.1021/acsami.6b06263

[14] Tseng YH, Yang H, Luo CW. Femtosecond laser-colorized indium-tin-oxide films for blue light attenuation and image screening. Optics Express.

2017;**25**:33134-33142. DOI: 10.1364/OE.25.033134

[15] Eichstät J, Römer GRBE, Huis AJ. Towards friction control using laser-induced periodic surface structures. Physics Procedia. 2011;**12**:7-15. DOI: 10.1016/j.phpro.2011.03.099

[16] Vorobyev AY, Guo C. Multifunctional surfaces produced by femtosecond laser pulses. Journal of Applied Physics. 2015;**117**:033103. DOI: 10.1063/1.4905616

[17] Vorobyev AY, Guo C. Metallic light absorbers produced by femtosecond laser pulses. Advances in Mechanical Engineering. 2010;**2010**:452749. DOI: 10.1155/2010/452749

[18] Vorobyev AY, Guo C. Enhanced absorptance of gold following multipulse femtosecond laser ablation. Physical Review B. 2005;**72**:195422. DOI: 10.1103/PhysRevB.72.195422

[19] Luo CW, Lee CC, Li CH, Shih HC, Chen YJ, Su CH, et al. Ordered YBCO sub-micron array structures induced by pulsed femtosecond laser irradiation. Optics Express. 2008;**16**:20610. DOI: 10.1364/OE.16.020610

[20] Guosheng Z, Fauchet PM, Siegman AE. Growth of spontaneous periodic surface structures on solids during laser illumination. Physical Review B. 1982;**26**:5366. DOI: 10.1103/PhysRevB.26.5366

[21] Donley C, Dunphy D, Paine D, Carter C, Nebesny K, Lee P, et al. Characterization of indium-tin oxide interfaces using X-ray photoelectron spectroscopy and redox processes of a chemisorbed probe molecule: Effect of surface pretreatment conditions. Langmuir. 2002;**18**:450-457. DOI: 10.1021/la011101t

[22] Szörényi T, Laude LD, Bertóti I, Kántor Z, Geretovszky Z. Excimer laser processing of indium-tin-oxide films: An optical investigation. Journal of Applied Physics. 1995;**78**:6211. DOI: 10.1063/1.360567

[23] Zhu F, Huan CHA, Zhang K, Wee ATS. Investigation of annealing effects on indium tin oxide thin films by electron energy loss spectroscopy. Thin Solid Films. 2000;**359**:244-250. DOI: 10.1016/S0040-6090(99)00882-2

[24] Fan JCC, Goodenough JB. X-ray photoemission spectroscopy studies of Sn-doped indium-oxide films. Journal of Applied Physics. 1977;**48**:3524-3531. DOI: 10.1063/1.324149

[25] Loeschner K, Seifert G, Heilmann A. Self-organized, gratinglike nanostructures in polymer films with embedded metal nanoparticles induced by femtosecond laser irradiation. Journal of Applied Physics. 2010;**108**:073114. DOI: 10.1063/1.3490191

[26] Elliott J, Smolyaninov II, Zheludev NI, Zayats AV. Polarization control of optical transmission of a periodic array of elliptical nanoholes in a metal film. Optics Letters. 2004;**29**:1414. DOI: 10.1364/OL.29.001414

[27] Chaney JA, Pehrsson PE. Work function changes and surface chemistry of oxygen, hydrogen, and carbon on indium tin oxide. Applied Surface Science. 2001;**180**:214-226. DOI: 10.1016/S0169-4332(01)00347-6

[28] Bonse J, Rosenfeld A, Krüger J. On the role of surface plasmon polaritons in the formation of laser-induced periodic surface structures upon irradiation of silicon by femtosecond-laser pulses. Journal of Applied Physics. 2009;**106**:104910. DOI: 10.1063/1.3261734

[29] Dufft D, Rosenfeld A, Das SK, Grunwald R, Bonse J. Femtosecond laser-induced periodic surface

structures revisited: A comparative study on ZnO. Journal of Applied Physics. 2009;**105**:034908. DOI: 10.1063/1.3074106

[30] Bonse J, Höhm S, Kirner SV, Rosenfeld A, Krüger J. Laser-induced periodic surface structures (LIPSS)—A scientific evergreen. IEEE Journal of Selected Topics in Quantum Electronics. 2016;**23**:9000615. DOI: 10.1364/CLEO_SI.2016.STh1Q.3

[31] Sipe JE, Young JF, Preston JS, van Driel HM. Laser-induced periodic surface structure. I. Theory. Physical Review B. 1983;**27**:1141. DOI: 10.1103/PhysRevB.27.1141

[32] Ray S, Banerjee R, Basu N, Batabyal AK, Barua AK. Properties of tin doped indium oxide thin films prepared by magnetron sputtering. Journal of Applied Physics. 1983;**54**:3497-3501. DOI: 10.1063/1.332415

[33] Konig TAF, Ledin PA, Kerszulis J, Mahmoud MA, El-sayed MA, Reynolds JR, et al. Electrically tunable plasmonic behavior of nanocube–polymer nanomaterials induced by a redox-active electrochromic polymer. ACS Nano. 2014;**8**(**6**):6182-6192. DOI: 10.1021/nn501601e

[34] Jaadane I, Boulenguez P, Chahory S, Carré S, Savoldelli M, Jonet L, et al. Retinal damage induced by commercial light emitting diodes (LEDs). Free Radical Biology and Medicine. 2015;**84**:373-384. DOI: 10.1016/j.freeradbiomed.2015.03.034